2021

CFD Simulation of Laminar Film Condensation on a Vertical Surface

David Vilar
University of Vigo, Spain

Elena Martín

Jaime Sieres
University of Vigo, Spain, jsieres@uvigo.es

CFD simulation of laminar film condensation on a vertical surface

David VILAR[1]*, Elena MARTÍN[1], Jaime SIERES[1]

[1] Departamento de Ingeniería Mecánica, Máquinas y Motores Térmicos y Fluidos
Escuela de Ingeniería Industrial, Universidade de Vigo
Campus Lagoas-Marcosende, 36310 Vigo – Spain
(Tel.: +34644237477, dvilar@uvigo.es)

* Corresponding Author

ABSTRACT

Two-dimensional simulations of laminar film condensation on a vertical surface are presented. A modified version of the **`interFoam`** solver present in OpenFOAM was developed, in order to take into account for energy and mass transfer. The Volume of Fluid (VOF) method is used to track the vapor-liquid interface, with the effects of interfacial stress, gravity and surface tension being considered.
Concerning the mass transfer model between phases, several models are used in the literature. Some authors have chosen empiric models, which incorporate some parameters that must be tuned by trial and error. The right estimate of those parameters is essential, since excessively high values lead to numerical convergence problems, while too small values cause a significant deviation between interfacial and saturation temperatures. The model used in this work forces the equilibrium state in the interface cells, in a dynamic way, which allows mesh independence to be achieved.
The obtained numerical results are compared against analytical results from Nusselt theory. The present numerical model is able to reproduce satisfactorily not only the Nusselt theory predictions, but additional effects (not included in that theory), namely, inertial forces, convective terms and interfacial shear stresses.

1. INTRODUCTION

Most of works of heat transfer in film condensation processes have been supported by theoretical and experimental studies. The most well-known work within the first group is the Nusselt theory (1916), who was the first to analyse the film condensation on a vertical wall. This work was a starting point for other authors, who made additional hypotheses, including convective terms, condensate subcooling or shear stress effects on condensate film (Rohsenow, 1956; Sparrow and Gregg, 1959; Chen, 1961). As the liquid film gets bigger, it becomes unstable. Small waves appear and grow rapidly until the turbulent regime flow is reached. During this transitional regime until reaching the turbulent film, Nusselt's theory is no longer valid. For this reason, the development of empirical or semi-empirical correlations was required for a more accurate calculation of heat transfer coefficients. Gichet and Jouhara (2019) present a complete review with some of the correlations existing in the literature, depending on the flow regime.
Although these correlations allow an easy calculation of the transferred heat, their validity can only be assured for the test conditions. Thanks to the development of Computational Fluid Mechanics (CFD) in recent years, numerical simulations are often carried out through the implementation of multiphase models. Simulations are presented in this paper using the Volume of Fluid (VOF) method (Hirt and Nichols, 1981), which can handle multiphase flows of immiscible fluids, tracking the motion of the interface between them without using empirical closure laws to model the interaction between the phases. Source terms must be included in the model to take into account mass transfer between phases. A number of papers use empirical expressions (Da Riva *et al., 2011;* Lee *et al.,* 2015; Yin *et al,* 2015) that contain parameters that need to be tuned by trial and error for each type of problem. This may be a limitation that we try to avoid in our work.
In the present work two dimensional simulations of laminar film condensation on a vertical surface are presented. An adaptation of the phase change model proposed by Rattner and Garimella (2014) has been carried out. The efficacy of this model is assessed by comparing the numerical results with theoretical data from Nusselt.

2. PHYSICAL SYSTEM AND COMPUTATIONAL METHODS

In this work laminar film condensation on a vertical plate and inside a vertical tube will be simulated. The physical systems to be considered in simulations are sketched in Figure 1. Vapor condensation occurs over a vertical surface maintained at T_w. The figure considers a situation where the vapor is at the saturation temperature T_s. Typical temperature profiles in the liquid film and vapor region are also indicated in the figure. Figure 1a) represents the case of stagnant vapor condensation on a vertical plate, while Figure 1b) represents the case of vapor condensation flowing inside a vertical tube.
In order to carry on the simulations the open-source software OpenFOAM was used. The VOF method was employed to track the interface. This method is implemented for multiphase incompressible flows in the solver *interFoam*. By taking as a basis this solver, the authors have modified it and created their own solver, *condensationFoam*, in which they have taken into account mass and energy transfer.

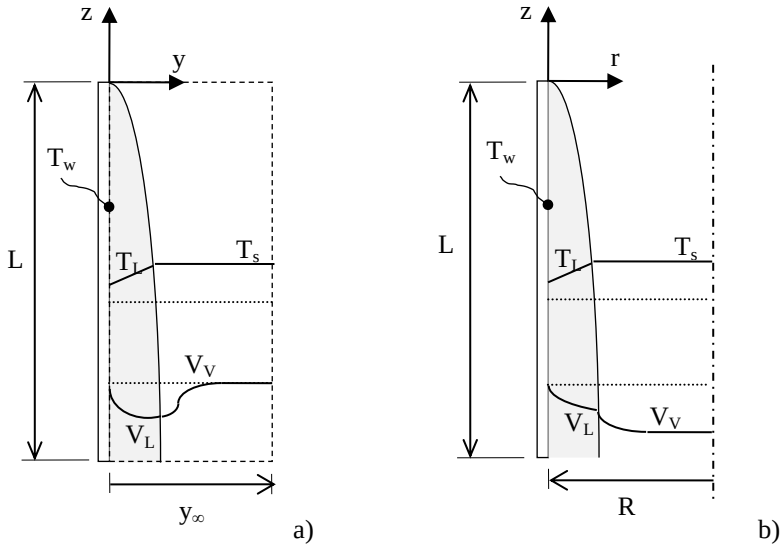

Figure 1: Schematic representation of the condensation section

2.1 VOF method

The VOF method is based on the definition of a volumetric fraction α, that represents the portion of the volume of the computational cell filled with one of the phases, generally liquid. In this method, the solution of the advection equation for the volumetric fraction is needed to track the interface:

$$\frac{\partial \alpha_L}{\partial t} + \nabla \cdot \left(\alpha_L \bar{V}\right) + \nabla \cdot \left[\overline{V}_c \alpha_L (1 - \alpha_L)\right] = \alpha_L \frac{\dot{\rho}}{\rho} \tag{1}$$

where $\dot{\rho}$ is the mass source term due to the phase change. This term will be discussed in the following section. This equation is numerically solved with the Multidimensional Universal Limiter for Explicit Evolution (MULES) scheme, which is an iterative implementation of the Flux Corrected Transport technique, used to guarantee boundedness in the solution of hyperbolic problems (Almeland, 2018). In this method it is not necessary the previous reconstruction of the interface, like in the Piecewise-Linear Interface Calculation (PLIC) scheme (Youngs, 1982). Thus the interface will have a finite width, so an additional term in (1) is required to compress it. This compressive term is the third one in the left hand side of (1), where $\overline{V}_c$ is the relative velocity between both phases. This variable depends on a parameter that can be tuned by the user.
As the VOF method considers the two-phase mixture as a single fluid, its properties are taken as a weighted mean depending on the volumetric fraction values for each cell. Then, once the interface position is updated in each temporal step, the thermophysical properties of the problem are calculated according to:

$$\psi = \psi_L \alpha_L + \psi_V (1 - \alpha_L) \tag{2}$$

where ψ applies to the density ρ, thermal conductivity k, viscosity μ and specific heat C_p.
These properties are considered to be constant in each phase and computed from the REFPROP database (Lemmon *et al.*, 2010).
Next, the momentum equation is solved by using the PISO (Pressure Implicit with Splitting of Operators) algorithm, to tackle pressure-velocity coupling. In PISO, an intermediate velocity field is first obtained, and the cell-face volume fluxes (ϕ) are evaluated and corrected for gravitational and surface forces and boundary conditions. Keeping in mind the non-divergence condition of the velocity field for the condensing flows investigated here ($\nabla \cdot \bar{V} = {\dot{\rho}}/{\rho}$), the Poisson equation for pressure can be written like this:

$$\nabla \cdot \left(\frac{1}{A_D} \nabla p_{rgh} \right) = \nabla \cdot \phi - \frac{\dot{\rho}}{\rho} \tag{3}$$

where A_D are the diagonal entries from the matrix momentum equation. After solving (3), the velocity field is corrected with the updated pressure field.
Finally the energy equation (4) is solved, and after that a new time step is calculated.

$$\frac{\partial (\rho c_p T)}{\partial t} + \bar{V} \nabla \cdot (\rho c_p T) = k \nabla^2 T + h_{LV} \dot{\rho} \tag{4}$$

2.2 Phase change model

In the literature several models for phase change can be found. The use of empirical expressions to determine mass and heat transfer at the interface is fairly widespread. The model proposed by Lee (1980) is one of the most used. This kind of models uses an empirical rate parameter that for different cases can have very dissimilar values (Wu *et al.*, (2007); Alizadehdakhel *et al.*, (2009)). Its value must be obtained from a trade-off between maintaining the temperature at the interface close to the saturation temperature and avoiding numerical divergence problems.
The phase change model used by the authors is based on the model presented in Rattner and Garimella (2014). This model does not require a geometric reconstruction of the interface. First, a mesh graph is generated in which the nodes and edges correspond to the cells and the faces of the mesh, respectively. Next, each pair of cells that contain the interface is identified. This is repeated at each time step. This way of proceeding is consistent with the notion of an infinitesimally thin interface, since as the mesh is refined, the volume of the cells of the interface will tend to 0. This is why a sufficiently fine mesh is required in the vicinity of the interface.
Once the interface cells have been defined, an initial nonlimited volumetric phase-change heating rate is evaluated for interface cells (5). This approach resembles the empirical rate parameter model proposed by Lee (1980). However, in the present model the phase-change heating rate is defined to force the interface to the saturation temperature at every time step, recovering the physical equilibrium condition. In Lee (1980) an empirical rate parameter is fixed and is independent of the simulation time step, so the interface temperature can diverge from the saturation temperature. Limiting must be applied to the initial phase-change heating rate (5), so that the amount of condensed mass in a cell does not exceed the amount of steam present in it (6), and it must also be satisfied that the speed of the steam entering a cell of the interface does not exceed the CFL (Courant-Friedrichs-Lewis) condition (7). This condition is ensured by limiting the local volumetric rate of volume sinking to $1/\Delta t$ (Rattner & Garimella, 2014). Thus, the phase-change heat rate will be the maximum of the three terms discussed above (8).

$$\dot{q}_{pc,0} = \frac{\rho c_p (T - T_{sat})}{\Delta t} \tag{5}$$

$$\dot{q}_{lim,mass} = -\frac{(1 - \alpha_L) \rho_V h_{LV}}{\Delta t} \tag{6}$$

$$\dot{q}_{lim,CFL} = -\frac{h_{LV}}{\Delta t} \left(\frac{1}{\rho_V} - \frac{1}{\rho_L} \right)^{-1} \tag{7}$$

$$\dot{q}_{pc} = max(\dot{q}_{pc,0}, \dot{q}_{lim,mass}, \dot{q}_{lim,CFL}) \tag{8}$$

Here, Δt is the simulation time-step value. It is worth to note that limiting terms (6-7) act effectively in the solver only for specific time steps at certain stages of the simulation but it is not the general rule in the simulation, where the phase-change heating rate is generally given by equation (5).

However, (8) constitutes a very localized term, concentrated just on interface cells. This has been proved to lead to numerical instabilities, given the high condensation rate concentrated in a few cells. To address this problem the work of Hardt and Wondra (2008) has been considered. Thus, the mass source term is smoothed, by solving a steady diffusion equation at every time step (9):

$$\nabla^2 \dot{\varphi} = \frac{1}{\Delta\tau D}(\dot{\varphi} - \dot{\varphi}_0) \tag{9}$$

where $\dot{\varphi}_0 = {\dot{q}_{pc}}/{h_{LV}}$ and $(\Delta\tau D)^{1/2}$ gives the length scale over which the original source-term is smeared ($1 \cdot 10^{-5}\ m$ for all simulations). From φ the final mass source term ($\dot{\rho}$) is obtained, accounting for mass creation on the liquid side of the interface, and vice versa on the vapor side. For more details, the reader is referred to Hardt and Wondra (2008).

2.3 Computational domain and boundary conditions

In this work, condensation on a vertical plate and inside a vertical tube was simulated, thus two different computational domains were used (Figure 1). In the first case, it is a rectangular two-dimensional domain with length 15mm and width 0.5mm. In the second case, a two-dimensional, axisymmetric domain is employed. Its length is set to 15mm, and the radius to 0.5mm. A quadrilateral mesh is adopted for the entire domain. The mesh size is uniform in the flow direction, whereas it is gradually refined near the wall. The size of cells close to the wall is 10 times smaller than that of the cells in the vapor freestream. In Table 1 the results from a grid independence analysis are presented, for a case of condensation of R134a on a vertical plate. Relative error is calculated by comparing the simulated heat flux with the Nusselt analytical heat flux.

Table 1: Grid sensitivity analysis for vapor condensation on vertical plate (R134a, $T_s - T_w = 10K$)

Number of cells	33750	67500	135000	270000
Relative error	0.037	0.0174	0.0192	0.0189

As can be seen in the Table 1, a good convergence is obtained for meshes with a number of cells greater than 67500 (relative error is below 2%). Thus, a mesh with 135000 quadrilateral elements was chosen to carry out the numerical computations presented in this paper.

One of the main problems in order to launch a simulation is initiating the liquid film. Thus a very thin liquid film of uniform thickness δ_o is applied to reduce the convergence time. The presence of this initial thickness also requires for certain velocity profiles to be obtained. Accordingly adiabatic simulations are previously launched in each case to get developed profiles to be used as a boundary condition at inlet. At the vapor inlet saturation temperature is imposed, while at the liquid inlet the temperature varies linearly from the wall temperature until saturation temperature. The walls are assumed to be isothermal, and at the outlet a pressure value is set, whereas a zero-gradient is imposed for the other variables. At the freestream boundary a zero-gradient condition is set for all variables (symmetry condition for the axisymmetric domain).

3. RESULTS

Numerical computations were performed using R134A and water as working fluids for the two configurations considered in Figure 1. In order to see effects not included in the Nusselt's theory, two simulations were launched with working fluids near their critical points. Table 2 resumes the basic data used for the different cases analyzed.

Table 2: Input data for the cases analyzed

Simulation	**Configuration**	**Working fluid**	**p_s (MPa)**	**T_{inlet} (K)**	**T_w (K)**	**$\overline{V_{inlet}}$ (m/s)**
VT134_1	Vertical tube	R134a	1.195	319.3	309.3	0.115
VT134_2	Vertical tube	R134a	1.195	319.3	309.3	0.335
VT134_3	Vertical tube	R134a	3.728	370	360	0.115
VPW_1	Vertical plate	Water	21.775	646	626	-
VP134_1	Vertical plate	R134a	1.195	319.3	309.3	-

Table 3 collects some relevant nondimensional parameters for each case.

Table 3: Nondimensional parameters for the cases analyzed

	VT134_1	**VT134_2**	**VT134_3**	**VPW_1**	**VP134_1**
Re_V	527	1535	1584	-	-
Pr_L	3.16	3.16	5.71	11.26	3.16
Ja_L	0.1	0.1	0.89	15.77	0.1
ρ_L/ρ_V	18.8	18.8	2.52	1.66	18.8

3.1 Stagnant condensation on a vertical plate

Results are presented for liquid film thickness, velocity and temperature fields for different axial positions ($\tilde{z}$). Additionally local Nusselt numbers at the wall are related to the film Reynolds number obtained at different vertical positions ($\tilde{y}$).

Figure 2 compares the numerical results for liquid film thickness with Nusselt prediction. It can be seen that results produced by our model fit well to those predicted analytically for both cases. For the case VPW_1, the amount of condensate deviates slightly from theory down the liquid film.

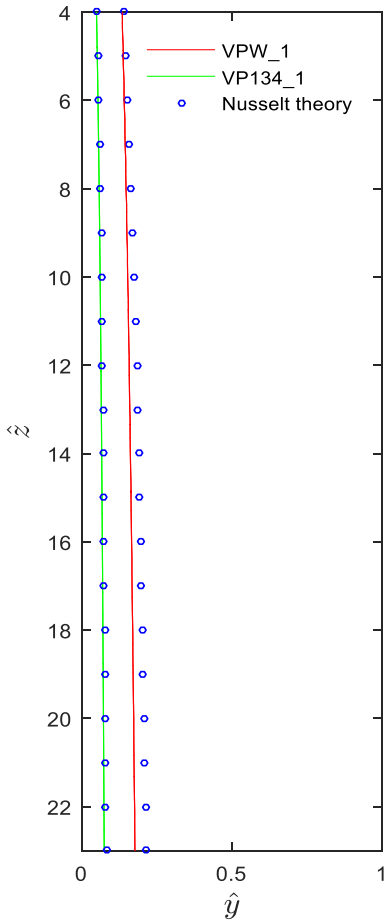

Figure 2: Comparison of film thickness given by numerical simulations and Nusselt's solution.

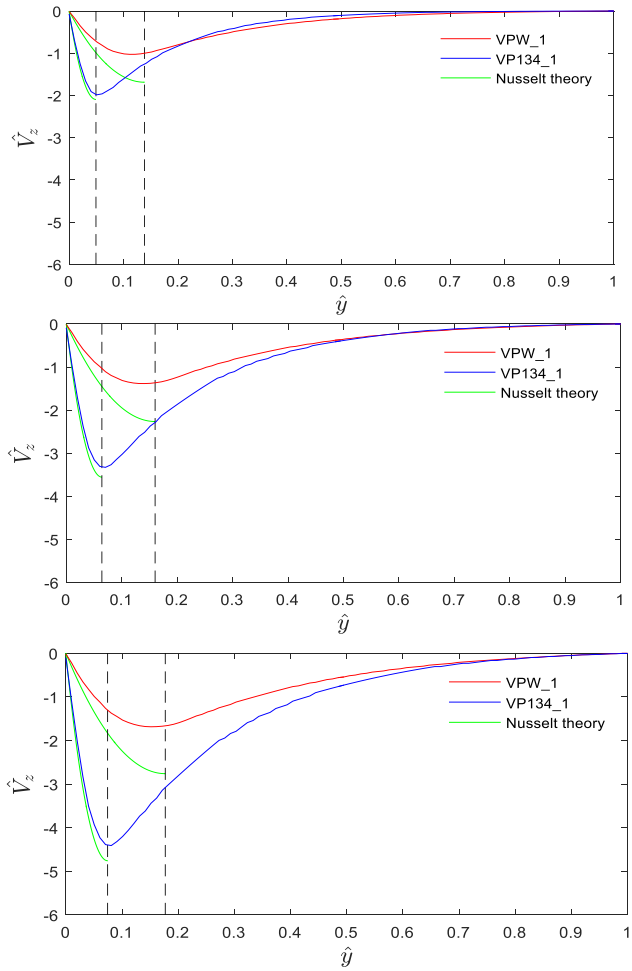

Figure 3: Comparison of axial velocity given by numerical simulations and Nusselt's solution, for $\tilde{z}$=4, $\tilde{z}$=10 and $\tilde{z}$=20, respectively, from top to bottom.

Figure 3 shows the non-dimensional vertical component of the velocity field at three vertical positions: $\tilde{z}$=4, $\tilde{z}$=10 and $\tilde{z}$=20. Liquid film mean velocity at $\tilde{z}$=2 was estimated to normalize the velocity field in each case. The dashed line shown in the figures indicate the position of the liquid-vapor interface. For comparison purposes the velocity profile predicted from the Nusselt theory is also represented. It can be seen that the film thickness increases with the vertical position, as the condensation process progresses. The velocity increases from the wall up to a maximum at the interface and then decreases in the vapor domain. Far away from the interface the vapor velocity approaches zero, in harmony with the imposed boundary condition. Whereas in case VP134_1 velocity doesn't move away so much from Nusselt prediction, in the case VPW_1 the classical theory clearly overestimates the liquid velocity. The liquid film drags the vapor and gives up some of its momentum. Therefore the film velocity decreases in comparison with theory, which doesn't take into account the effects of inertia forces, convection term and interfacial shear stress.

Figure 4 shows the non-dimensional temperature distribution at $\tilde{z}$=10 for both cases. Numerical results for R134a fit the linear curve predicted by Nusselt, which means that conductive heat transfer prevails in the liquid film. For the water case, the temperature curve becomes slightly parabolic. It seems clear that convective effects are important. In this case, the Prandtl number for water is three times that of R134a.

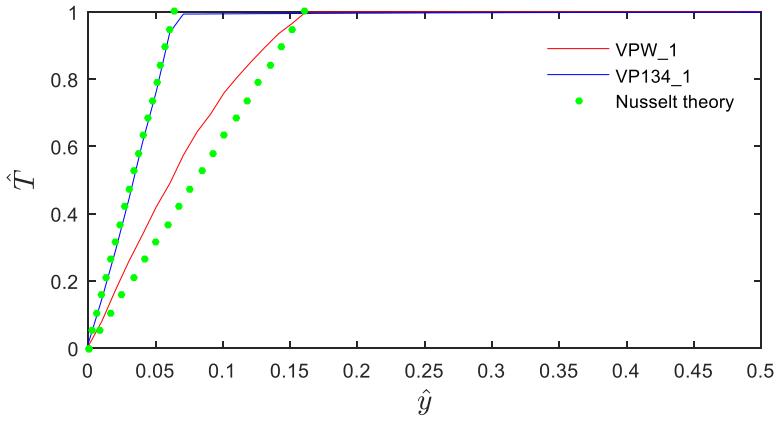

Figure 4: Comparison of temperature field given by numerical simulations and Nusselt's solution, for $\tilde{z}$=10.

For the purpose of numerically analyzing the heat transfer features of the condensation process and its comparison with the Nusselt theory, the local Reynolds and Nusselt numbers for the liquid film along the vertical wall are calculated as follows:

$$Re_z = \frac{4\Gamma_z}{\mu_L} \tag{10}$$

$$Nu_z = \frac{q_z''}{(T_s - T_w)\, k_L} \left(\frac{\mu_L^2}{\rho_L(\rho_L - \rho_V) g} \right)^{1/3} \tag{11}$$

where Γ_z is the condensate mass flow rate per unit width of surface and it is determined by:

$$\Gamma_z = \rho_l \int_0^{\delta_z} v_z(y,z)\, dy \tag{12}$$

In Figures 5 and 6, the calculated local Nusselt numbers are shown as a function of the Reynolds number along the vertical wall. It can be seen that both Nusselt numbers decrease monotonically with the Reynolds number. Results in Figure 5 also show very good agreement of the model with the predictions obtained by the classical Nusselt theory, i.e.:

$$Nu_z = \left[\frac{\rho_L(\rho_L - \rho_V) g h_{LV} z^3}{4 k_L \mu_L (T_s - T_w)} \right]^{1/4} = 1.1\, Re_z^{-1/3} \tag{13}$$

In Figure 6 the numerical results are significantly higher than those obtained by the expression (13). Several reasons are behind this fact. Sparrow & Gregg (1959) or Chen (1961) revisited the Nusselt's theory adding some effects ignored in it, such as inertial forces, convective terms or interfacial shear stresses. They proved that, for practical values of Pr_L and Ja_L, classical theory is perfectly valid. When these two parameters reach abnormally high values, Nusselt's theory gives underestimated values for heat transfer. For water near the critical point (VPW_1) these parameters are very high (11.3 for Prandtl number and 15.8 for Jakob number, from Table 2). Therefore we can assume that we are in the aforementioned situation, so it seems reasonable that heat transfer is higher than Nusselt's predictions. In the same way, Rohsenow (1956) corrected the latent heat in (13) in order to take into account the liquid subcooling, by using a simple expression:

$$h_{LV}^{*} = h_{LV}\left[1 + \frac{3}{8}\left(\frac{c_{pL}(T_S - T_W)}{h_{LV}}\right)\right] = h_{LV}\left(1 + \frac{3}{8}Ja_L\right) \tag{14}$$

A new correction for latent heat was proposed by Rohsenow (1956) and Bromley (1952), allowing the temperature profile in liquid film to be non-linear:

$$h_{LV}^{*} = h_{LV}(1 + 0.68Ja_L) \tag{15}$$

Expression (13) is shown in Figure 6 corrected by (14) and (15). It is seen that numerical results agree well with expressions (14) and (15). Correction (15) fits better at the beginning of the film, while (14) at the end. This may be because the amount of condensate deviates slightly from what is expected in theory (Figure 2).

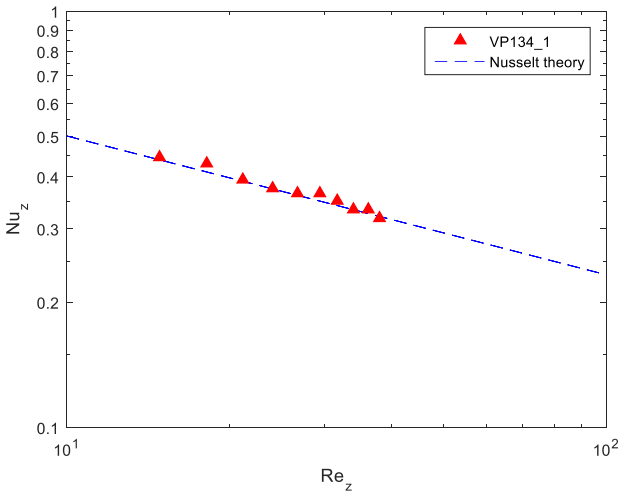

Figure 5: Local Nusselt number as a function of Reynolds number at different axial positions. Comparison with theoretical results from Nusselt.

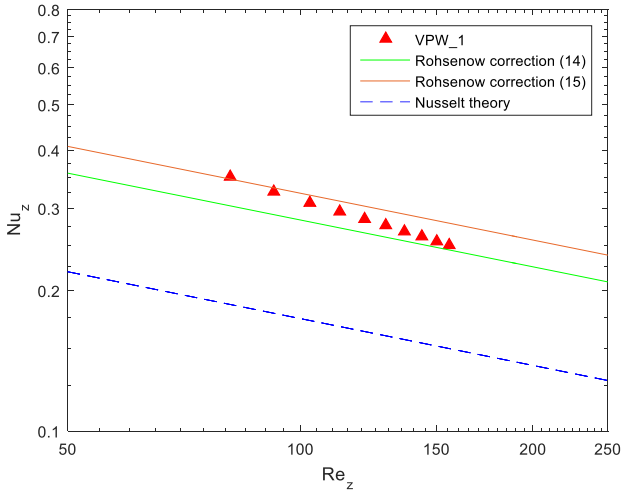

Figure 6: Local Nusselt number as a function of Reynolds number at different axial positions. Comparison with theoretical results from Nusselt and Rohsenow correction.

3.2 Vapor condensation flowing inside a vertical tube

The following section presents the numerical results of the condensation of R134a inside a vertical tube, with a length equal to 30 times the radius. First, the distribution of the non-dimensional axial velocity at different vertical positions is shown in Figures 7-9, for cases VT134_1-3, respectively. Inlet vapor mean velocity was used to normalize the velocity field in each case. In the first one, it is observed that as the condensate film thickness (liquid-vapor interface represented by black dots) increases, the vapor gives part of its momentum to the liquid. At the outlet the condensate film drags the vapor, since the highest velocity in the vapor domain is reached in the vicinity of the interface, while it is almost negligible in the rest of the domain. Case VT134_2 is represented in Figure 8. Here the vapor enters with a higher velocity than before ($Re_V \approx 1535$), so the velocity variations in the vapor domain are much smaller than in the previous case. It can be seen that vapor drags the liquid film along the entire length. In case VT134_3 (Figure 9) vapor enters the domain with certain velocity ($Re_V \approx 1584$). The condensation rate is higher than in the previous case.

For the purpose of analyzing the heat transfer features the expressions (11)-(14) used in the previous section continue to be valid. Although they are given for condensation on vertical plate, their use is also recommended for condensation inside vertical tubes, unless the tube inside diameter is very small and tube wall curvature effects become important (Marto, 1998). Otherwise, theoretical results from Nusselt should be revisited (Le *et al.*, 2014). In Figure 10 numerical results are compared against (13). In case VT134_1, with a moderate vapor entry velocity, numerical results approach well to (13), as expected. When increasing the vapor flow at inlet (VT134_2) the drag force on the liquid film along the entire length also increases, but only slightly differences are appreciated at the tube inlet. In the third case (VT134_3), differences with respect to the theory are significant. For this case, Prandtl and Jakob number are greater than in cases before, so it is expected that heat transfer results given by the Nusselt theory are underestimated. The numerical results agree well with the Rohsenow correction (15).

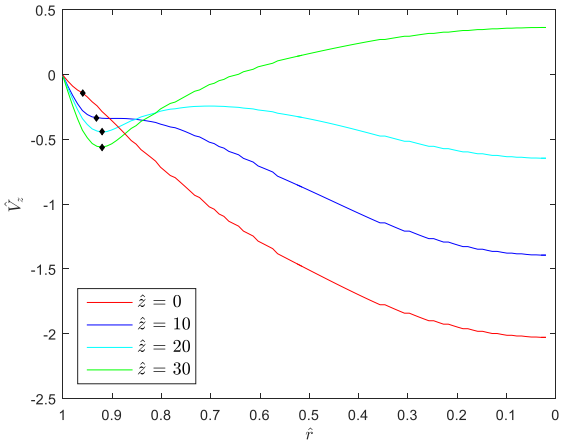

Figure 7: Axial velocity distribution at different pipe sections, for the case VT134_1. Black dots represent the position of the liquid-vapor interface.

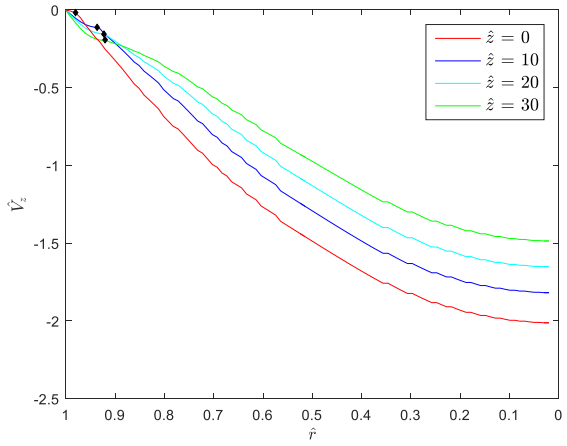

Figure 8: Axial velocity distribution at different pipe sections, for the case VT134_2. Black dots represent the position of the liquid-vapor interface

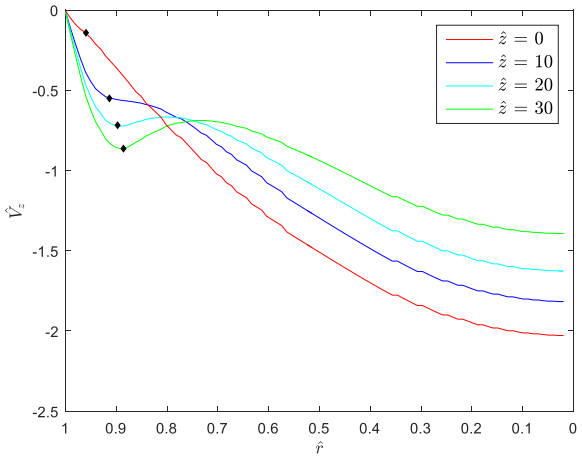

Figure 9: Axial velocity distribution at different pipe sections, for the case VT134_3. Black dots represent the position of the liquid-vapor interface

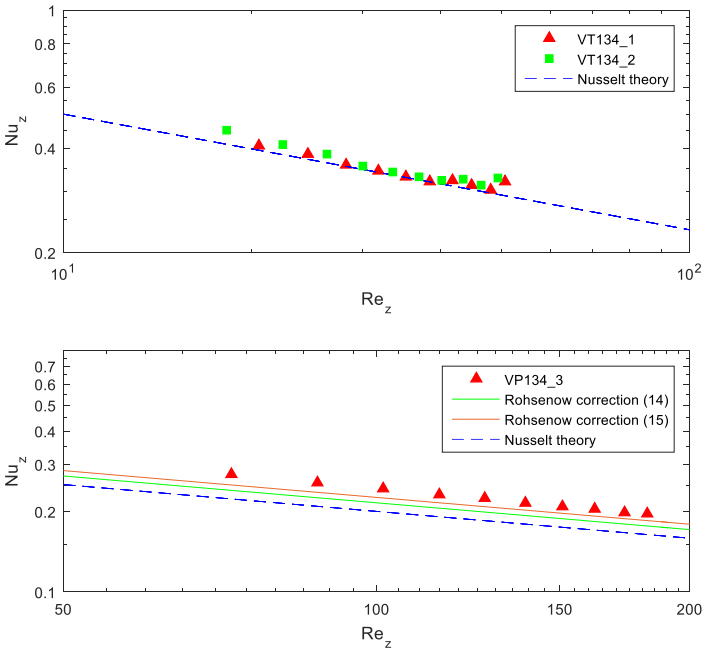

Figure 10: Local Nusselt number as a function of Reynolds number at different axial positions.

4. CONCLUSIONS

Two-dimensional simulations of laminar film condensation on vertical surfaces have been presented. Stagnant condensation on a vertical plate and condensation of flowing vapor inside a vertical pipe have been considered. The VOF method was used to track the liquid-vapor interface.

A new solver for condensation, *condensationFoam*, was developed by the authors. The phase change model was adapted from the model proposed by Rattner and Garimella (2014). Its performance was evaluated by comparing against the Nusselt theory. Numerical results obtained for vertical plate were quite accurate and fitted well with the theory. Some effects not included in the theory were presented, like convective effects, not negligible for high Prandtl and Jakob numbers. For condensation inside a vertical tube different cases were launched, depending on the inlet vapor mass flow and on the saturation temperature. All of them are in accordance with the classical theory.

NOMENCLATURE

A_D	diagonal matrix of momentum equation	(kg m^{-3} s^{-1})
c_p	isobaric specific heat	(J kg^{-1} K^{-1})
D	tube diameter	(m)
g	gravity acceleration	(m s^{-1})
h_{LV}	latent heat	(J kg^{-1})
Ja	Jakob number, $c_p(\mathrm{T_s} - \mathrm{T_w})/h_{LV}$	(-)
k	thermal conductivity	(W m^{-1} K^{-1})
L	plate or tube length	(m)
Nu	condensation Nusselt number	(-)
$\dot{q}_{pc,0}$	non-limited volumetric phase change heating rate	(kg m^{-1}s^{-3})
p	pressure	(Pa)
p_{rgh}	dynamic pressure, $p - \rho g z$	(Pa)
Pr	Prandtl number, $c_p\mu/k$	(-)
q''	heat flux	(W m^{-2})
r	r-coordinate	(m)
$\tilde{r}$	non-dimensional r-coordinate, r/R	(-)
R	tube radius	(m)
Re	liquid film Reynolds number	(-)
Re_V	inlet vapor Reynolds number, $\rho_V V D/\mu_V$	(-)
t	time	(s)
T	temperature	(K)
$\tilde{T}$	non-dimensional temperature, $\frac{T-T_w}{T_s-T_w}$	(-)
V	velocity	(m s^{-1})
V_c	relative velocity	(m s^{-1})
$\tilde{V}$	non-dimensional velocity, $V/\bar{V}$	(-)
y	y-coordinate	(m)
y_∞	width of the simulation domain	(m)
$\tilde{y}$	non-dimensional y-coordinate, y/y_∞	(-)
z	z-coordinate	(m)
$\tilde{z}$	non-dimensional z-coordinate, z/y_∞ or z/R	(-)
Greek symbols		
α	volume fraction	(-)
μ	dynamic viscosity	(Pa s)
ϕ	cell face volumetric flux	(m s^{-1})
Γ	condensate mass flow rate	(kg m^{-1} s^{-1})
ρ	density	(kg m^{-3})
$\dot{\rho}$	phase change mass source	(kg m^{-3} s^{-1})
$\dot{\varphi}$	smeared phase change mass source	(kg m^{-3} s^{-1})
δ_0	initial film thickness	(m)

Subscripts

L	liquid
V	vapor
w	wall
s	saturation
i	interface
z	local values along axial direction

REFERENCES

Alizadehdakhel, A., Rahimi, M., Alsairafi, A.A., (2010). CFD modelling of flow and heat transfer in a thermosyphon. *International Communications in Heat and Mass Transfer*, 37, 312-318.

Almeland, S.K.. (2018). Implementation of an air-entrainment model in interFoam. In Nilsson, H. (Ed.) *Proceedings of CFD with OpenSource Software*, http://dx.doi.org/10.17196/OS_CFD#YEAR_2018

Bromley, L.A., (1952). Heat transfer in condensation – Effect of heat capacity of condensate. *Ind. Eng. Chem.,* 44, 12, 2966-2969.

Chen, M. M., (1961). An analytical study of laminar film condensation: Part 1 – Flat plates, *Trans. ASME, J. Heat Transf.,* 83, 48-54.

Da Riva, E., Del Col, D., (2011). Effect of gravity during condensation of R134a in a circular minichannel. VOF simulation of annular condensation. *Microgravity Sci. Technol.,* 23 (Suppl 1):S87-S97.

Guichet, V., Jouhara, H., (2020). Condensation, evaporation and boiling of falling films in wickless heat pipes (two-phase closed thermosyphons): A critical review of correlations. *International Journal of Thermofluids,* 1-2, 100001.

Hardt, S., Wondra, F., (2008)., Evaporation model for interfacial flows based on a continuum-field representation of the source terms. *Journal of Computational Physics,* 227, 5871-5895.

Hirt, C. W., Nichols, B. D., (1981). Volume of Fluid (VOF) method for the dynamics of free boundaries. *Journal of computational physics,* 39, 201-225.

Marto, P.J., (1998). Condensation. In Rohsenow, W.M., Hartnett, J.P., Cho, Y.I. (Eds.), *Handbook of heat transfer* (Chapter 14), 3rd Edition. McGraw-Hill.

Le, Q. T., Ormiston, S.J., Soliman, H.M., (2014). A closed-form solution for laminar film condensation from quiescent pure vapours on curved vertical walls. *International Journal of Heat and Mass Transfer*. 73, 834-838.

Lee, W.H., (1980). A pressure iteration scheme for two-phase flow modelling. In Verizoglu, T.N. (Ed.), *Multiphase Transport Fundamentals, reactor safety, applications*, vol.1, Hemisphere Publishing, Washington DC.

Lee, H., Kharangate, C.R., Mascarenhas, N., Park, I., Mudawar, I., (2015). Experimental and computational investigation of vertical downflow condensation. *International Journal of Heat and Mass Transfer*, 85, 865-879.

Lemmon, E., Huber, M., McLinden, M.O., (2010). REFPROP (Reference Fluid Thermodynamic and Transport properties), NIST Standard Reference Database 23.

Nusselt, W., (1916). Die oberflachenkondensation des Wasserdampfes. *Z. Ver. Deut. Ing.*, 69, 541-546.

Rattner, A.S., Garimella, S., (2014). Simple mechanistically consistent formulation for Volume-of-Fluid based computations of condensing flows. *Journal of Heat Transfer*, July 2014, Vol. 136

Rohsenow, W.M., (1956). Heat transfer and temperature distribution in laminar-film condensation. *Trans. ASME*, 78, 1645-1648.

Sparrow, E.M., Gregg, J.L., (1959). A boundary layer treatment of laminar film condensation. *Trans. ASME, J. Heat Transf.,* 81, 13-18.

Wu, H.L., Peng, X.F., Ye, P., Gong, Y., (2007). Simulation of refrigerant flow boiling in serpentine tubes. *Int. J. Heat Mass Transfer*, 50, 1186-1195.

Yin, Z., Guo, Y., Sunden, B., Wang, Q., Zeng, M., (2015). Numerical simulation of laminar film condensation in a horizontal minitube with and without non-condensable gas by the VOF method. *Numerical Heat Transfer, Part A*, 68, 958-977.

Youngs, D.L., (1982). Time-dependent multi-material flow with large fluid distortion. In: *Numerical Methods for Fluid Dynamics*, Academic Press, New York.